Nonlocal effects in the electron-positron interaction in metals

A. Rubaszek
W. Trzebiatowski Institute of Low Temperature and Structure Research, Polish Academy of Sciences, P.O. Box 1410, 50-950 Wrocław 2, Poland

Z. Szotek and W. M. Temmerman
Daresbury Laboratory, Daresbury, Warrington, WA4 4AD, Cheshire, United Kingdom

(Received 11 September 2000; revised manuscript received 20 December 2000; published 5 April 2001)

We study the importance of the nonlocal electron-positron interaction for positron annihilation characteristics in simple and transition metals. This is accomplished by using the weighted density approximation, giving rise to nonlocal and energy-dependent electron-positron correlation functions. We apply this formalism to study the momentum-dependent and momentum-averaged electron-positron enhancements of the positron annihilation rates and the three-dimensional electron-positron momentum densities. The results of the present approach are compared to those obtained within the local density approximation, generalized gradient approximation, Bloch modified ladder approximation, and experimental data. We find that while nonlocality of the electron-positron correlations is of substantial importance for the core and *d* electrons in transition metals, for nearly-free-electron bands the energy dependence of the electron-positron correlation functions is of more significance.

DOI: 10.1103/PhysRevB.63.165115 PACS number(s): 78.70.Bj, 71.60.+z

I. INTRODUCTION

Positron annihilation spectroscopies are very useful for studying electronic structure of solids, and in particular, the electron momentum density (EMD).[1,2] Unfortunately, the latter, as measured by the positron annihilation techniques, is modified by both positron charge distribution and strong electron-positron (e-p) attraction. The effect of the electron-positron attraction, leading to the formation of an electron screening cloud around the positron, can be adequately represented by the so-called electron-positron enhancement factor. It is defined as a ratio of the e-p annihilation rate to its independent particle model (IPM) counterpart. This e-p enhancement factor, together with the positron charge distribution, are the two ingredients that are indispensible for the interpretation of the positron annihilation data, in terms of the electron momentum distribution. The usefulness of the information recovered from the positron annihilation data is crucially dependent on the accuracy of the e-p correlation functions that give rise to the e-p enhancement factors. Of course, the e-p correlation functions, giving account of the many-body e-p interactions, depend both on the positron position and the initial electron Bloch state. This can also be seen from angular correlation of positron annihilation radiation (ACAR) data. When interpreting their ACAR spectra for simple metals, Stewart and co-workers[3] concluded that the e-p enhancement factors in the first Brillouin zone (BZ) were strongly momentum dependent. This strong momentum dependence of the e-p enhancement factors translates directly into a strong energy dependence of the e-p correlation functions and was extensively studied in Refs. 3–11. Important conclusions concerning the e-p correlation functions could also be drawn from the interpretation of the two-dimensional (2D) ACAR spectra in transition metals[6,12] by fitting to the theoretically derived, momentum-dependent, Kahana-like e-p enhancement factors.[13] This led to the observation of negative slopes of the momentum-dependent enhancement factors for *d* electrons, implying a strong position dependence of the e-p correlation functions. Nevertheless, in most theoretical calculations of the positron annihilation characteristics in metals, the position dependence of the e-p correlation functions has been either neglected[4,6] or included only locally.[9,12,14] Most recently the nonlocal effects of the e-p correlation functions have been studied, for instance, in Refs. 8, 11, and 15.

In the present paper we apply the nonlocal and energy-dependent approach of the weighted density approximation[11] (WDA) to study the e-p momentum densities and band-decomposed e-p enhancement factors in simple and transition metals. Among all metals we have studied, detailed discussion of the e-p momentum distributions and momentum dependent enhancement factors is presented only for the simple fcc metal Al and two 3*d* transition metals, Cu and V, which crystallize, respectively, in the fcc and bcc structures. Cu is a classical 3*d* system that has been most thoroughly studied both theoretically and experimentally, and is therefore an ideal benchmark for an assessment of any new methodology. Aluminum serves a similar purpose, but on the more free-electron-gas-like side. Regarding V, it has been chosen mainly because it is a bcc system, but also because there exist results in literature that we can compare against while discussing the importance of the nonlocal effects for the positron annihilation characteristics.

The remainder of the paper is organized as follows. In the next section, we briefly present the theoretical background for calculating the e-p correlation functions, and with these functions the e-p momentum densities and enhancement factors. In Sec. III, the results for the positron lifetimes, average, and total e-p enhancement factors, and momentum densities are presented and discussed in detail for Al, Cu, and V, in comparison with other theoretical calculations by means of the local density approximation (LDA), nonlocal generalized gradient approximation[15] (GGA), Bloch modified ladder

(BML) approximation,[8] and experiments.[1,16–18] We conclude the paper in Sec. IV.

II. THEORY

The e-p momentum density, $\rho(\mathbf{p})$, is calculated as[1,2]

$$\rho(\mathbf{p}=\mathbf{k}+\mathbf{G}) = \sum_j \rho_j(\mathbf{p}) = \sum_{\mathbf{k}j}^{occ} \left| \sum_l \int_\Omega e^{-i\mathbf{p}\cdot\mathbf{r}} \psi_+(\mathbf{r}) \psi^l_{\mathbf{k}j}(\mathbf{r}) \sqrt{\gamma^l_{\mathbf{k}j}(\mathbf{r})}\, d\mathbf{r} \right|^2, \tag{1}$$

where $\mathbf{p}$ is the electron momentum in the extended zone scheme, and $\mathbf{G}$ is the reciprocal lattice vector. The angular momentum, l, decomposed electron wave functions, $\psi^l_{\mathbf{k}j}(\mathbf{r})$, with the wave vector $\mathbf{k}$ and band index j, are calculated within the local density approximation to density functional theory (DFT),[19] using the linear muffin-tin orbitals (LMTO) band structure method with the atomic sphere approximation (ASA).[20] To improve on the ASA, in the present calculations of $\rho(\mathbf{p})$ we have implemented also the Jarlborg-Singh correction.[12] For the core electrons, the frozen core approximation has been used. The wave function, $\psi_+(\mathbf{r})$, of a thermalized positron in its ground state, is the solution of the Schrödinger equation, with the positron potential consisting of the external potential due to ions, the Hartree potential, and the e-p correlation (V_{corr}) potential. The latter, describing the positron interaction with the electron screening cloud, can be determined from the Feynmann theorem.[11,14,21,22] The positron Hartree and external potentials are equal to the respective electron potentials, but with the opposite sign.

The state-dependent two-particle e-p correlation function, $\gamma^l_{\mathbf{k}j}(\mathbf{r})$, is defined as a ratio of the angular-momentum- and state-resolved electron charge density, at the positron position $\mathbf{r}$, to the corresponding quantity in the absence of a positron. The e-p correlation function accounts for the fact that when positron enters a solid a polarization cloud is formed, as a result of which the densities of the individual electron states, $\mathbf{k}j$, at the positron position $\mathbf{r}$, become strongly enhanced with respect to their initial values. This e-p correlation function, combined with the electron charge density, gives rise to the so-called e-p momentum-dependent enhancement factor

$$\epsilon(\mathbf{p}) = \rho(\mathbf{p})/\rho^{IPM}(\mathbf{p}),$$

where $\rho^{IPM}(\mathbf{p})$ is the e-p momentum density calculated within the independent particle model. The e-p momentum-dependent enhancement factor may be further decomposed into the individual band contributions

$$\epsilon_j(\mathbf{p}) = \rho_j(\mathbf{p})/\rho^{IPM}_j(\mathbf{p}),$$

which are useful quantities for a detailed analysis of the positron annihilation results.

In most theoretical approaches to the e-p correlations in real solids, use is made of the e-p enhancement factors for the homogeneous electron gas (of density n_0), $\epsilon^h(|\mathbf{k}|,n_0)$. In the LDA, the correlation functions, $\gamma^l_{\mathbf{k}j}(\mathbf{r})$, are approximated by the respective quantities for the homogeneous electron gas,[13,23] $\gamma^h_{\mathbf{k}j}(n(\mathbf{r}))$, with the local electron density, $n(\mathbf{r})$, at the positron position $\mathbf{r}$. In this approach, the e-p correlation functions, $\gamma^l_{\mathbf{k}j}(\mathbf{r})$, are approximated by the energy-dependent Kahana-like e-p enhancement factors, $\epsilon^h(E_{\mathbf{k}j}/E_F, n(\mathbf{r}))$, as proposed in Refs. 4 and 9, with $E_{\mathbf{k}j}$ being the electron eigenvalues in the initial state $\mathbf{k}j$ and E_F the Fermi energy. Within the LDA one can define both the state-independent (see, e.g., Refs. 12, 14, 15 and 21) and state-dependent[9,10] correlation functions, but they are always local quantities. To take into account nonlocal effects, beyond the LDA description, Barbiellini *et al.*[15,24] used a parameter-dependent, GGA-type approach and defined the nonlocal, but state-independent, correlation functions. Using the weighted density approximation, Rubaszek *et al.*[11] determined both the state-dependent and nonlocal correlation functions, $\epsilon^h(E_{\mathbf{k}j}/E_F, \tilde{n}_l(\mathbf{r}))$, which, unlike the LDA correlation functions, depend on the angular momentum decomposed effective electron density, $\tilde{n}_l(\mathbf{r})$, in the whole space. Details on calculating the WDA e-p correlation functions, which will be used in this paper, can be found in Ref. 11.

To finish this section, let us define two additional quantities that will be used in the next section. The first, introduced by Genoud *et al.*,[6] is a semiempirical, $\mathbf{r}$-independent, but angular-momentum-resolved and energy-dependent e-p correlation function of the form[4,13]

$$\overline{\gamma}^l_{\mathbf{k}j} = a_l + b_l E_{\mathbf{k}j}/E_F + c_l (E_{\mathbf{k}j}/E_F)^2. \tag{2}$$

The angular-momentum-dependent parameters a_l, b_l, and c_l have been obtained by fitting the product of Eq. (2) and the IPM momentum density to the experimental 2D ACAR spectra. In what follows, whenever appropriate, we shall compare our results for the e-p momentum distributions and enhancement factors in V and Cu to the corresponding semiempirical quantities, calculated according to Eqs. (1) and (2) using the parameters a_l, b_l, and c_l determined in Ref. 6.

The second quantity, which we shall refer to while discussing our results, is the momentum-averaged, but angular-momentum-decomposed, e-p enhancement factor

$$\Gamma_l = \lambda_l/\lambda^{IPM}_l, \tag{3}$$

defined as a ratio of the angular-momentum-decomposed annihilation rate, λ_l, to its IPM equivalent, λ^{IPM}_l. Summing up the former over the angular momentum l gives the total annihilation rate λ as

$$\lambda = \pi r_0^2 c \frac{\Omega}{(2\pi)^3} \int \rho(\mathbf{p})\, d\mathbf{p} = \sum_l \pi r_0^2 c \int |\psi_+(\mathbf{r})|^2 \sum_{\mathbf{k}j}^{occ} [|\psi^l_{\mathbf{k}j}(\mathbf{r})|^2 \gamma^l_{\mathbf{k}j}(\mathbf{r})]\, d\mathbf{r} = \sum_l \lambda_l, \tag{4}$$

with Ω, r_0, and c being, respectively, the volume of the sample, the classical electron radius, and the velocity of light. The inverse of λ defines the positron lifetime τ.

III. RESULTS AND DISCUSSION

In this section, we study the influence of the state-dependent and nonlocal two-particle correlation function, $\gamma_{\mathbf{k}j}(\mathbf{r})$, on a variety of positron annihilation characteristics in metals. We present results for the angular-momentum-decomposed average enhancement factors and positron lifetimes for a large cross section of metals. Moreover, we discuss in detail the importance of the nonlocal effects for the e-p momentum densities on the example of Al, Cu, and V. Both valence and core electrons are considered. In addition, the momentum-dependent enhancement factors are analyzed in terms of individual electron bands. Wherever possible, we compare our calculations against the experimental data or semiempirical results.

In what follows we present calculations for the positron annihilation characteristics, performed within the nonlocal and state-dependent WDA approach, and compare them to the LDA results. The latter may appear as either state-dependent LDA results, where the energy-dependent enhancement factors, $\epsilon^h(E_{\mathbf{k}j}/E_F, n(\mathbf{r}))$ [selective enhancement factor (SEF)] are used, or as the state-independent LDA results, utilizing the constant enhancement factors (CEF). We shall refer to these two different LDA results, respectively, as LDA-SEF and LDA-CEF. Additionally, to illustrate the importance of the state selectivity of the two-particle e-p correlation functions, $\gamma_{\mathbf{k}j}(\mathbf{r})$, we compare the WDA results to another nonlocal, but state-independent, approach, namely GGA. Finally, we also discuss comparison of the WDA results with those of the BML approach, which is both nonlocal and state-selective.

A. Average enhancement factors and positron lifetimes

In order to get a general feeling for the importance of the nonlocal effects, in Fig. 1 we display the average enhancement factors, $\Gamma_{s,p,d+f}^{WDA(LDA)}$ [see Eq. (3)], for various angular-momentum channels and a substantial cross section of simple and transition metals. It can be seen that the average WDA enhancement factors for s and p electrons, $\Gamma_{s(p)}^{WDA}$'s, are slightly larger than, but otherwise very similar to, their LDA counterparts, $\Gamma_{s(p)}^{LDA}$'s, implying that for the nearly free electrons the nonlocal e-p correlation effects are of no significance. In contrast, for d and f electrons in transition metals the nonlocal effects are seen to substantially alter the resulting enhancement factors. Indeed, the distributions of the d- and f-electron contribution to the electron screening cloud around the positron differ considerably between the WDA and LDA approaches.[11] The d (f) part of the electron screening charge distribution, calculated within WDA, is shifted with respect to its LDA counterpart from the positron position towards the intermediate region of the Wigner-Seitz sphere, where d and f electrons reside, while the positron distribution has the highest weight in the interstitial region. Consequently, the values of Γ_{d+f}^{WDA}'s are considerably smaller

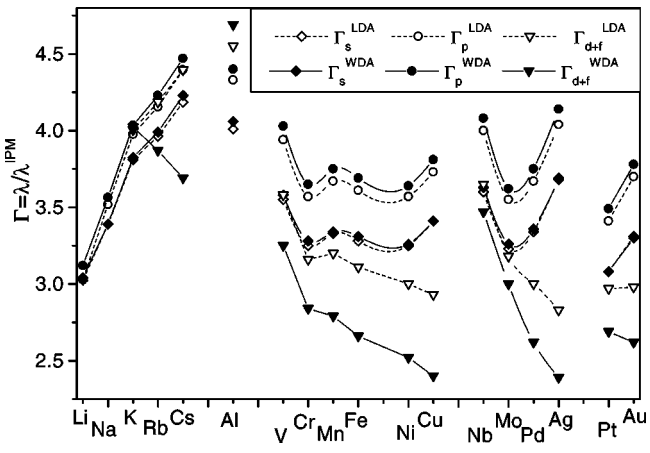

FIG. 1. Average enhancement factors for s, p, and $d+f$ electrons. The connecting lines serve only as a guide for eyes. The superscript in Γ defines the approximation used for the e-p correlation functions in Eq. (4), while the subscript refers to the type of electrons. Note that to fit the values of the alkali metals in the figure, the cubic root of Γ's, with a prefactor of 1.5, has been plotted.

than those of Γ_{d+f}^{LDA}'s, indicating that the nonlocal correlation effects are crucial for the calculations of the positron annihilation characteristics in transition metals. Note that for any of the $3d$, $4d$, and $5d$ metal series, differences between the WDA and LDA results increase with filling up the respective d shells. Although similar trends in $\Gamma_d^{WDA(LDA)}$ are also observed in alkali metals, the d-electron contribution to the positron annihilation rates in these systems is almost negligible.

As can be seen in Fig. 2, also positron lifetime, τ, captures the above features of the average WDA enhancement factors. For all d electron metals WDA gives higher positron lifetimes, and with the exception of Nb and Mo, leads to better agreement with experiments.[25,26] In simple metals, the nonlocal effects do not alter much the valence electron contribution to the total lifetime. Therefore, the observed increase of the WDA positron lifetimes in K and Rb, as compared to LDA, seems to be mainly due to a large core electron contribution.

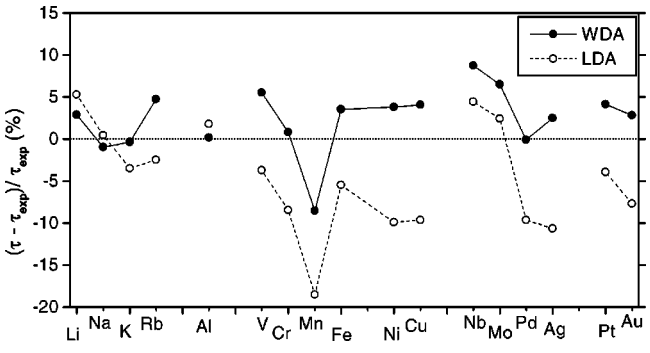

FIG. 2. The relative percentage deviations in the calculated positron lifetimes with respect to experimental values for a variety of metals. The experimental values for V, Cr, Fe, Ni, Cu, Pd, and Ag come from Ref. 26, and for other metals from Ref. 25.

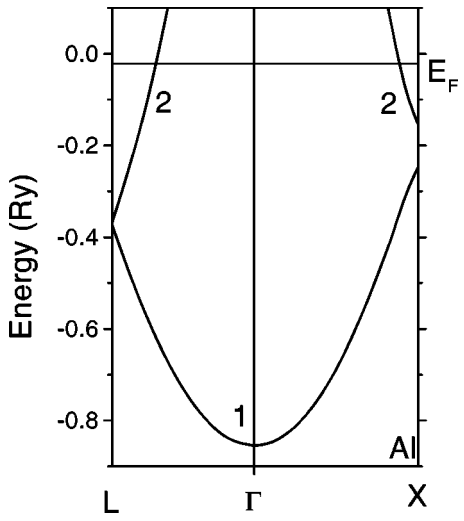

FIG. 3. The annihilation active energy bands in Al along two crystallographic directions in the {001} plane.

Finally, the nonlocal e-p interaction effects should, in principle, be reflected differently for different types of electrons in the corresponding momentum-dependent annihilation characteristics, $\epsilon(\mathbf{p})$ and $\rho(\mathbf{p})$. Since the e-p momentum density $\rho(\mathbf{p})$ is a representation of hybridized s-, p-, d-, and f-electron bands, one can expect that for any momentum $\mathbf{p}$, deviations between WDA and LDA partial annihilation rates (or e-p enhancement factors) should provide reliable information on the degree of d and f character in the electron bands contributing to the EMD in the host material.

B. Aluminum

Before discussing the calculated positron annihilation characteristics let us start with the band structure of Al, shown in Fig. 3, which is a very important input to the calculations. In aluminum three valence electrons fill completely the first and partially the second band, marked in the figure respectively by 1 and 2. Both bands are sp-like, with a very small admixture of d character. Therefore, the nonlocal e-p interaction effects are not expected to make a big impact on the calculated e-p momentum densities and enhancement factors in the first BZ. The same should be true up to the Fermi momentum in the second BZ, as the partially occupied second band, which is also free-electron-like, provides the main contribution to $\rho(\mathbf{p})$ in this region. This nearly-free-electron character of the occupied valence bands is reflected in the positron annihilation characteristics, shown in Figs. 4 and 5. In these figures we compare results of different approximations, namely WDA, LDA, and GGA, with the experimental data and the results of a semiempirical analysis by Nakashima *et al.*,[17] for, respectively, [100] and [111] directions. These semiempirical results were obtained by combining the IPM momentum densities with the Kahana-like enhancement factor of the form

$$\epsilon(\mathbf{p}) = a + b[\mathbf{p}/\mathbf{p}_F]^2 + c[\mathbf{p}/\mathbf{p}_F]^4, \tag{5}$$

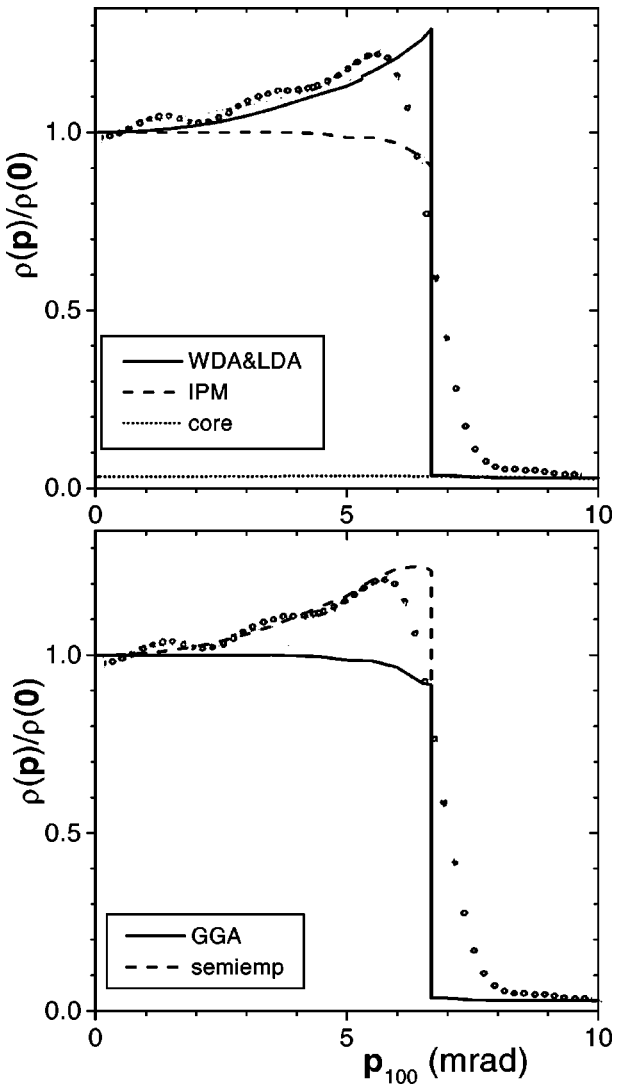

FIG. 4. Electron-positron momentum densities for Al along the [100] direction, calculated within WDA, LDA-SEF, and GGA, and compared to the semiempirical and experimental results. All the spectra are normalized to unity at $\mathbf{p}=0$ and the momenta are expressed in milliradians. In the upper panel the core electron contribution is also shown.

where $\mathbf{p}_F$ is the Fermi momentum. The parameters a, b, and c were determined individually for the three main crystallographic directions by fitting the resulting values of $\rho(\mathbf{p})$ to 3D reconstructed ACAR spectra.

Looking at Fig. 4, where the e-p momentum densities along [100] direction are displayed, one can see that up to the Fermi momentum $\mathbf{p}_F$, the WDA and LDA-SEF e-p momentum densities are almost identical. Moreover, the high-momentum components (HMC's) of the valence contribution to $\rho(\mathbf{p})$ are very small, confirming that the d-electron character in the electron wave function is almost negligible. The nonlocal e-p interaction effects hardly influence the resulting e-p momentum densities in the whole momentum space. The e-p momentum densities, calculated within the state-dependent approaches of WDA and LDA, have a Kahana-like increasing slope, which is typical for an electron

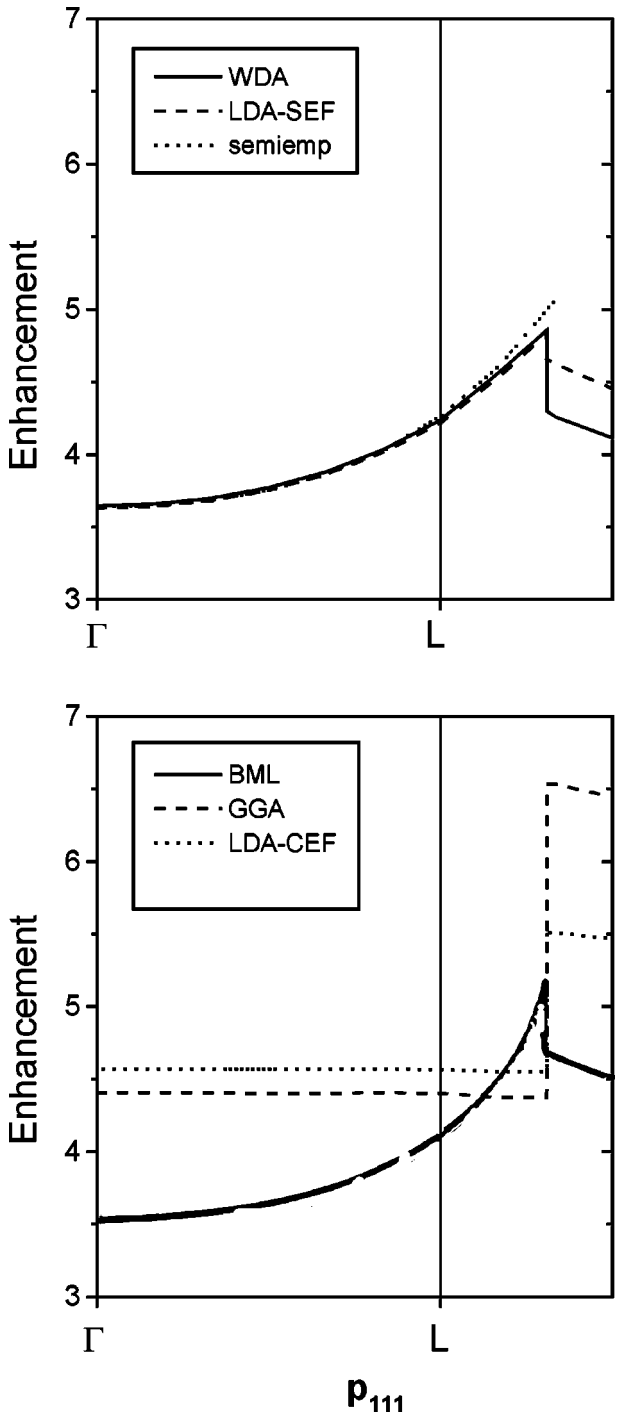

FIG. 5. Momentum-dependent total enhancement factors $\epsilon(\mathbf{p})$, calculated for Al within various approximations along the [111] direction.

gas.[13,23,27] Also, as can be seen in the lower panel of Fig. 4, the experimental ACAR spectra, corresponding to the central Fermi surface (FS), are well described by the biparabolic Kahana form of Eq. (5). Note further that, the LDA and WDA e-p momentum densities are slightly less increasing functions of momentum than the respective semiempirical curves. A possible reason for this may be the isotropic character of the jellium enhancement factors, used in the WDA and LDA calculations, since the experimental data show some anisotropy.[13,23,27] The e-p momentum density of the nonlocal, but state-independent, approach of GGA is very IPM-like and, as much as the IPM result, does not agree with the experimental data for all values of momentum up to the Fermi momentum $\mathbf{p}_F$. This implies that the state-dependent two-particle correlation functions are essential for the realistic calculation of the positron annihilation characteristics in simple metals, at least as far as the central FS is concerned.

In Fig. 5 we display the total e-p enhancement factors, $\epsilon(\mathbf{p})$, along the [111] direction. Similarly to the [100] direction, the WDA and LDA-SEF results are very much the same up to the Fermi momentum $\mathbf{p}_F$, and agree well both with the semiempirical enhancement factor and the BML result. The situation is less favorable for the state-independent approaches of GGA and LDA-CEF, which give rather constant enhancement factors up to the Fermi momentum. Moreover, in spite of nearly-free-electron-like character of valence bands in Al, the nonlocality of the GGA correlation functions gives rise to a considerable reduction of the relevant enhancement factors with respect to their local counterparts, for momenta inside the central FS. Outside the central FS, the presence of the nonlocal e-p interaction effects in the e-p enhancement factors is much more apparent, due to predominantly d character of $\rho(\mathbf{p})$. It is puzzling, however, that in this region of space the results of the two nonlocal approaches, namely WDA and GGA, exhibit dramatically different trends: The WDA enhancement factors, $\epsilon(\mathbf{p})$, are reduced with respect to the LDA-SEF quantities, while the GGA enhancement factors are considerably larger than the LDA-CEF results. In the case of WDA, such a reduction seems quite obvious. Since the d-electron contribution dominates in the e-p momentum density, WDA would naturally deliver reduced values of the e-p correlation functions in Eq. (1), in agreement with the nonlocal approach of BML. The situation does not seem to be as obvious regarding GGA, and to understand the two different trends one should refer to the experimental ACAR spectra, which unfortunately show rather low intensity in the high-momentum region.

Finally, it is interesting to note that in Al *overenhancement*, $\epsilon(\mathbf{k}+\mathbf{G})>\epsilon(\mathbf{k})$ for $\mathbf{G}\neq\mathbf{0}$, is observed in the high-momentum region. This *overenhancement* is markedly stronger for the state-independent approaches of GGA and LDA-CEF than for the WDA, LDA-SEF, and BML approaches. The WDA, LDA-SEF, and BML curves show qualitatively very similar slopes along the [111] direction, with the nonlocal effects observed in the whole umklapp region.

In summary, the nonlocal effects do not seem to be of much importance for the positron annihilation characteristics in simple metals like Al, at least for momenta inside the central FS. The state dependence of the two-particle correlation functions appears to be by far most important here. The nonlocal effects start to play some role in the high-momentum region where, however, the intensity of the high-momentum components in the EMD and e-p momentum density is very small.

C. Copper

Here we present the WDA results for Cu for both the e-p momentum densities and momentum-dependent enhance-

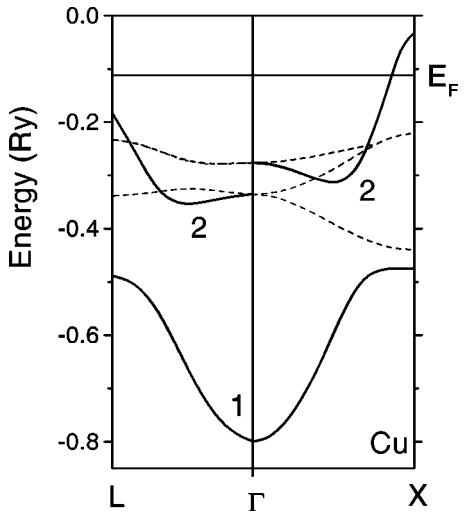

FIG. 6. Energy bands in Cu along two crystallographic directions in the {001} plane. The solid curves denote the annihilation active bands, while the dashed curves indicate the inactive bands.

ment factors, and compare them to the present and earlier LDA calculations, GGA,[15] and BML[8] results, as well as to the experimental[1,16,28] and semiempirical data.[4,6] Such comparisons are expected to shed light on the importance of the nonlocal e-p correlations and the state selectivity of the e-p correlation functions for the calculation of the positron annihilation characteristics in d electron metals.

As can be seen in Fig. 6, in Cu, due to symmetry-related selection rules,[29] there are only two totally or partially occupied valence bands that contribute to the electron and e-p momentum densities. These bands are marked by digits 1 and 2 and in the following text will be referred to as the first and second bands. Both of them have strongly hybridized sp- and d-like character, which is reflected accordingly in momentum densities $\rho(\mathbf{p})$ shown in Figs. 7 and 8, respectively along the [100] and [111] directions, and calculated within various approximations. In the upper panels of Figs. 7 and 8, the core electron contribution to $\rho(\mathbf{p})$ is also shown. The first thing to note in Fig. 7 is that the two independent experimental spectra,[1,16] collected by two different groups, have very similar shapes, thus indicating high-quality 3D reconstructions (in Ref. 16 the 2D ACAR measurements were carried out for as many as 10 projections). Regarding the theoretical results, close to the Γ point, for small values of $|\mathbf{p}|$, both LDA and WDA are very much the same, which reflects the fact that in this region the contribution of the upper d-like band to $\rho(\mathbf{p})$ is negligible, while the lower band has nearly-free-electron-like character. When the momentum $|\mathbf{p}|$ increases towards the BZ boundary, the contribution of the second band increases, while the first band becomes more d-like in character. Therefore, in this region the experimental spectra show an increasing slope, followed closely by the LDA and WDA curves. When the d-electron contribution to the annihilation characteristics increases, the difference between the WDA and LDA results becomes more apparent, with the WDA curves becoming less momentum-dependent functions, improving agreement with experiments. Note, that the nonlocal effects reduce considerably the two-particle correlation functions, $\gamma^d_{\mathbf{k}j}(\mathbf{r})$, in the region where the d electron density has the largest overlap with the positron distribution.[11]

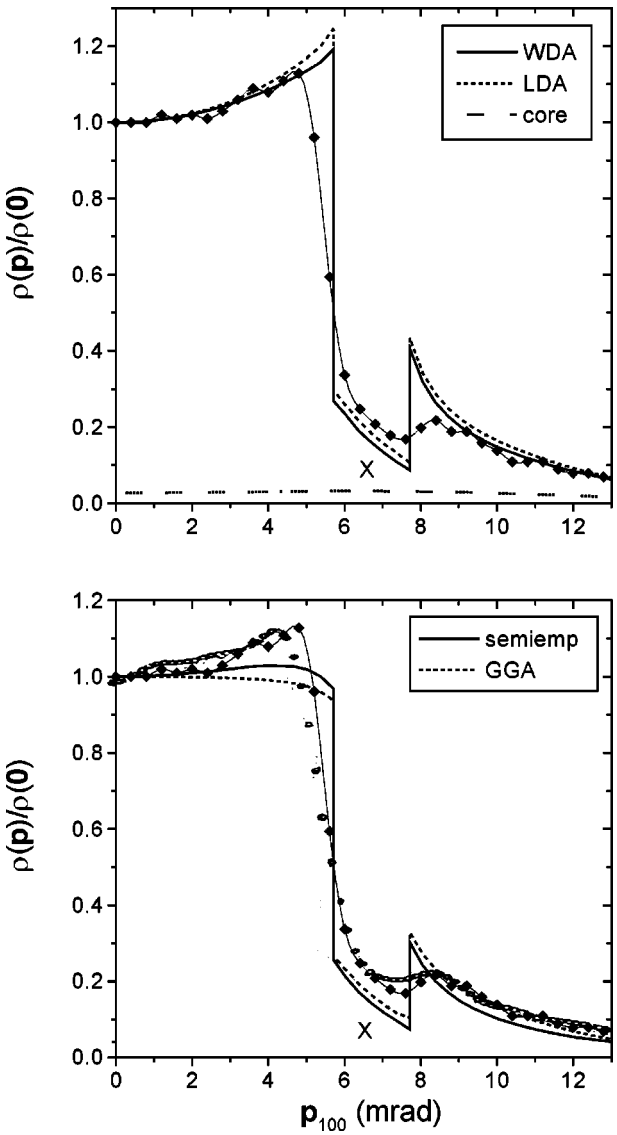

FIG. 7. Electron-positron momentum densities for Cu along the [100] direction, calculated within WDA, LDA-SEF, and GGA, compared to the semiempirical and experimental results. In the upper panel the core electron contribution is also shown. The solid diamonds and open circles denote the experimental 3D spectra, reconstructed respectively in Refs. 1 and 16. The semiempirical results have been obtained according to Eqs. (1) and (2), with the parameters $a_s=a_p=1$, $a_d=0.9$, $b_s=b_p=0.1$, $b_d=0$, $c_s=c_p=0$, and $c_d=-0.5$, as determined in Ref. 6.

Moving to the bottom panel of Figs. 7 and 8, one can see that GGA, which is not state-selective, leads to almost constant $\rho(\mathbf{p})$ for all momenta in the central FS, and therefore does not reproduce the observed behavior of the experimental curves. This indicates that in this region of momentum space not only the nonlocality, but also state selectivity of the correlation functions, is essential for the calculation of realistic ACAR spectra. With respect to the semiempirical results, obtained using the SEF-type correlation functions,

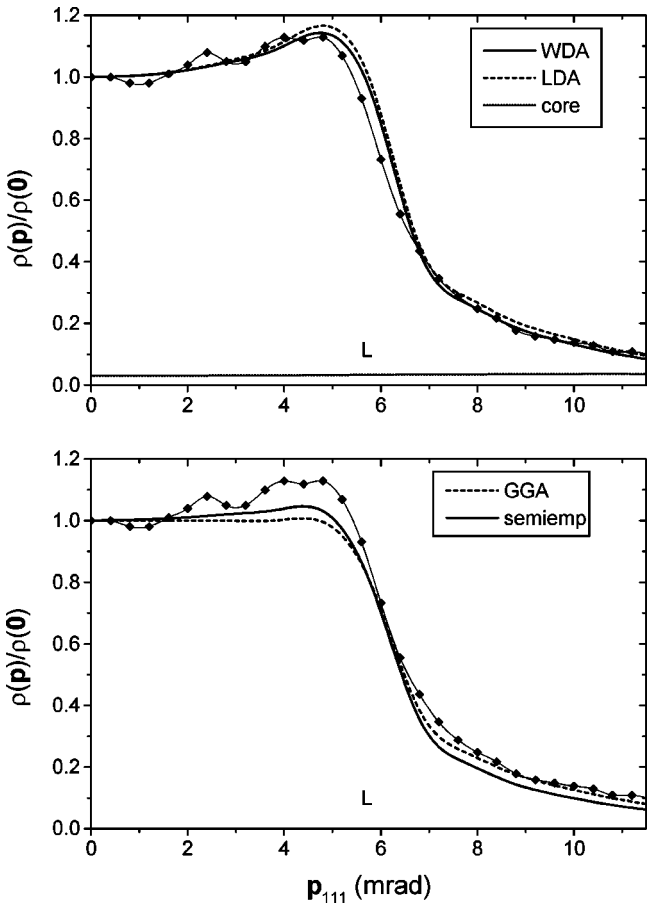

FIG. 8. Electron-positron momentum densities for Cu along the [111] direction, calculated within WDA, LDA-SEF, and GGA, compared to the semiempirical and experimental results. In the upper panel the core electron contribution is also shown. The solid diamonds denote the experimental 3D spectra reconstructed in Ref. 1. The semiempirical results have been obtained according to Eqs. (1) and (2), with the parameters $a_s=a_p=1$, $a_d=0.9$, $b_s=b_p=0.1$, $b_d=0$, $c_s=c_p=0$, and $c_d=-0.5$, as determined in Ref. 6.

they show slightly increasing slopes. However, for momenta greater than 3 mrad, the semiempirical spectrum and the ''true'' experimental data differ quite substantially. The reason could be that the fitted value of the c_d parameter for d electrons [see Eq. (2) and the captions of Figs. 7 and 8] is too negative, leading to a considerable underestimation of the d-electron enhancement factor.

Focusing on discontinuities in $\rho(\mathbf{p})$ along the [100] direction, which are clearly visible in the first and second BZ's, one can see that all calculated curves, shown in Fig. 7, intersect the experimental curves approximately at half maximum, and this is independent of the approximation used for the e-p correlation functions in Eq. (1). However, the GGA and semiempirical curves cross the experimental spectrum twice, because their slopes become negative when approaching the Fermi momentum. According to the Majumdar's theorem,[30] the positions of the FS breaks are a unique characteristic of the electronic structure of the host material, and cannot be shifted by either positron distribution or e-p interaction effect. Therefore, although the position of the intersection point of the theoretical and experimental curves is a good test of quality of the underlying electronic structure and 3D experimental reconstruction, it cannot serve as a severe test of quality of the approximation used for the e-p correlation functions entering Eq. (1).

Note that in the vicinity of the X point (Fig. 7), where only the first, d-like, band contributes to $\rho(\mathbf{p})$, all curves, both theoretical and experimental, have very similar negative slopes, although the theoretical curves lie below the experimental spectra. This seems to suggest that all approximations used in the present study underestimate the e-p correlation effects. It is also possible that the relative proportions of the s and d characters in the LDA electron wave function differ substantially from those of the true electron quasiparticle wave function, thus contributing to the observed differences. In addition, the finite resolution of the 2D ACAR apparatus is also an important factor here. In the high-momentum region, on the other hand, the agreement between theory and experiment is much more satisfactory. There, both along the [100] and [111] directions, mostly d electrons contribute to $\rho(\mathbf{p})$, and therefore the nonlocal approaches of WDA and GGA provide the best representation for the e-p momentum densities.

In order to illustrate the importance of both the nonlocality and state selectivity of the two-particle e-p correlation functions, in Figs. 9 and 10 we display the band-decomposed relative enhancement factors, $\epsilon_j(\mathbf{p})/\epsilon(\mathbf{0})$, reflecting the character of a given energy band j, for both annihilation active bands along the [111] direction. Starting with Fig. 9 and the first band, one can see that as long as the nearly-free-electron character of the band dominates, the WDA and LDA-SEF enhancement factors, $\epsilon_1(\mathbf{p})$, are almost indistinguishable, exhibiting the Kahana-like increasing slopes. A similar behavior is observed in the BML and semiempirical curves, although the latter, presumably due to the choice of $c_s=c_p=0$ in Eq. (2), is a less increasing function of momentum. Regarding the GGA and LDA-CEF, they remain fairly constant functions of momentum, implying that the state selectivity of the two-particle correlation functions is important. With increasing momentum towards the BZ boundary, all enhancement factor curves acquire a negative slope, indicating a predominantly d-like character of the band. Note that the nonlocal approaches lead to more pronounced negative slopes. For the second annihilation active band (Fig. 10), the negative slopes of the WDA, BML, and semiempirical enhancement factors, $\epsilon_2(\mathbf{p})$, in the vicinity of the Γ point, reflect its d character. Towards the BZ boundary, where this band becomes more sp-like, the WDA, BML, and LDA-SEF enhancement factors increase with momentum, with the latter resembling the Kahana-like behavior. However, the semiempirical enhancement factor decreases monotonically towards the BZ boundary, which again is presumably caused by a particular choice of the $c_{s,p}$ parameters. Regarding the GGA and LDA-CEF curves, they remain fairly constant in the first BZ, with a moderate rise towards the BZ boundary. Outside the central FS, all curves acquire negative slopes when moving towards the Γ' point and beyond, implying d character of the high-momentum components in $\rho(\mathbf{p})$. Note that in the high-momentum region the effect of nonlocality

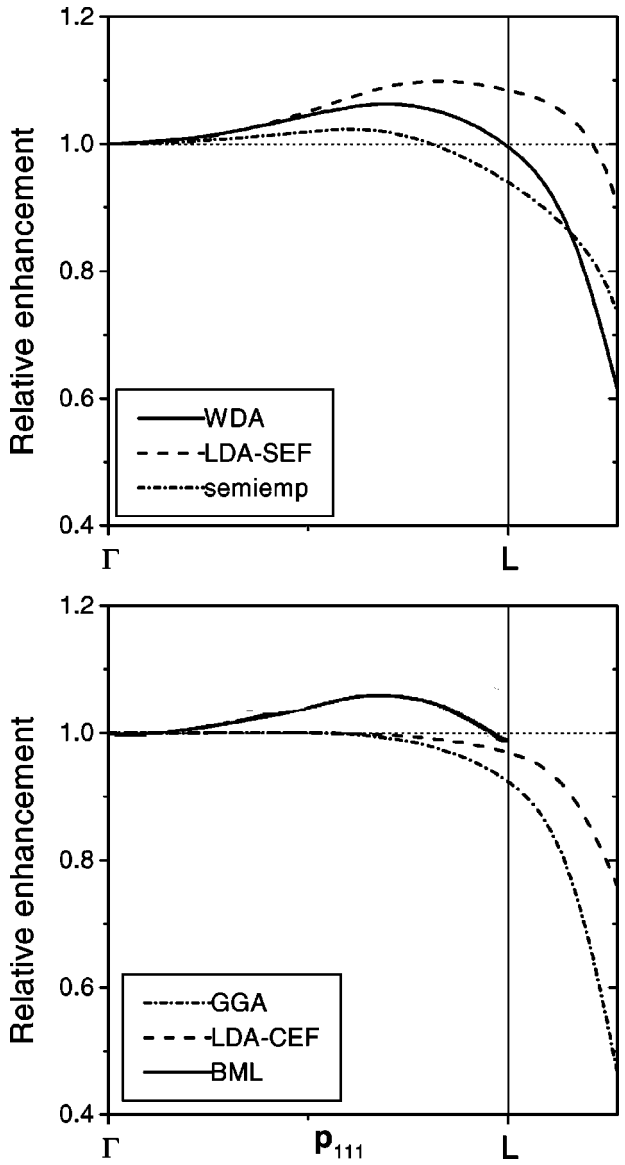

FIG. 9. Momentum-dependent relative enhancement factors for the first annihilation active band, $\epsilon_1(\mathbf{p})/\epsilon(\mathbf{0})$, calculated within various approximations for Cu along the [111] direction.

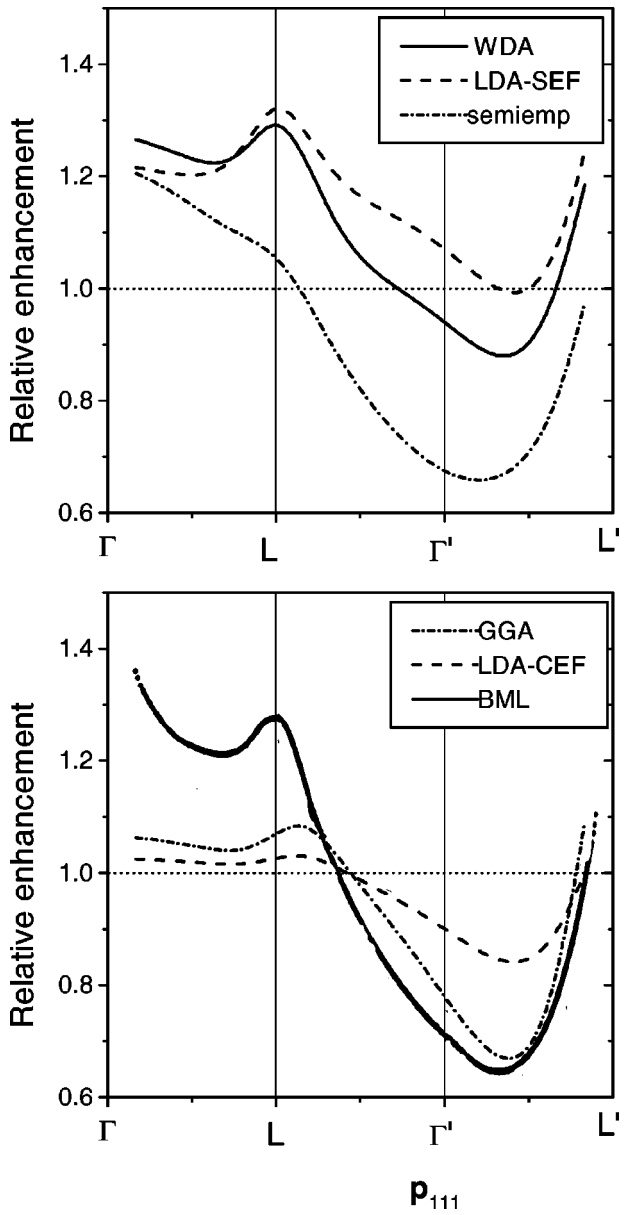

FIG. 10. Momentum-dependent relative enhancement factors for the second annihilation active band, $\epsilon_2(\mathbf{p})/\epsilon(\mathbf{0})$, calculated within various approximations for Cu along the [111] direction.

of the *e-p* correlations is much more pronounced in the respective enhancement factors than it was the case in the low-momentum region. Note also, that in all theoretical curves *deenhancement*, $\epsilon(\mathbf{k}+\mathbf{G})<\epsilon(\mathbf{k})$ for $\mathbf{G}\neq\mathbf{0}$, is seen in the high-momentum region. This *deenhancement*, first observed experimentally,[31] seems to be more pronounced in the curves originating from the nonlocal approaches.

Concluding this subsection, it suffices to say that the nonlocal *e-p* correlation effects can be clearly observed in the positron annihilation characteristics in the region where the *d*-electron character dominates. In such a case, the nonlocality of the two-particle correlation functions suppresses the importance of the state selectivity. When the electron bands are nearly-free-electron-like, then the nonlocal effects hardly matter, and it is the state selectivity of the *e-p* interaction that plays the most important role.

D. Vanadium

As can be seen in Fig. 11, in V the upper (*d*-like) annihilation active bands are either completely unoccupied or only a tiny fraction of them dips below the Fermi level. The resulting *e-p* momentum densities $\rho(\mathbf{p})$, shown in Figs. 12 and 13, respectively, along [100] and [110] directions, are much less influenced by *d* electrons than in the case of Cu. Indeed, as can be seen in Fig. 12, for small values of momentum $\mathbf{p}$ (up to 3.5 mrad), the WDA, LDA, and semiempirical momentum densities show very similar increasing slopes, reflecting the nearly-free-electron character of the only contributing band in this region. The GGA, on the other hand, is very IPM-like, while the experimental curve[18] shows strong oscillations, which could be ascribed to a propagation of the correlation noise in the reconstruction process. This

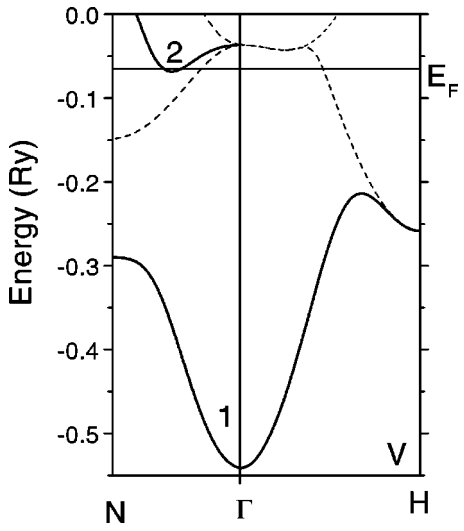

FIG. 11. Energy bands in V along two crystallographic directions in the {001} plane. The solid curves denote the annihilation active bands, while the dashed curves indicate the inactive bands.

oscillatory behavior is in variance to the character of more recent 3D momentum density reconstructed by Kubota *et al.*,[32] which appears to be a much stronger increasing function of momentum, providing support to the present results of the state-dependent approaches of WDA and LDA. Unfortunately, more quantitative comparison with the 3D data of Kubota *et al.*[32] would only be possible if one managed to read off the experimental points from the graph of their paper. For values of momentum greater than 4.0 mrad, where the character of the band switches over to predominantly *d*, both the theoretical and experimental momentum densities are decreasing functions of momentum, and the experimental and semiempirical densities are almost indistinguishable. There exists good agreement between the WDA, LDA, and the experimental full widths at half maximum (FWHM), although the WDA momentum density shows slightly sharper structure than the LDA curve. The reason for the sharper structure is that in this region the *d*-electron contribution dominates in the positron annihilation characteristics. However, a noticeable difference can be observed between the FWHM of the GGA momentum density and the corresponding experimental and semiempirical quantities. In fact the GGA result is difficult to reconcile with either the semiempirical or experimental momentum density in the whole momentum range. This is because the state dependence of the two-particle correlation functions, not taken into account within GGA, matters here even more than their nonlocality.

In the [110] direction, the *e*-*p* momentum densities show a very interesting structure, which arises from dipping of the second band below the Fermi level (see Fig. 11). It can be seen in Fig. 13 that the theoretical curves show several prominent peaks and valleys, which indicate the occupation of the second band. In the region of the ''spikes'' one can observe noticeable differences between the WDA and LDA momentum densities that can be ascribed to a predominantly *d* character of the second band. In this region WDA reduces the *e*-*p* correlation effects, as compared to LDA, and improves the agreement with the semiempirical result. The GGA momentum density curve does not reproduce the shape of the semiempirical data, either for the first or second band. In general, unlike in the [100] direction, the comparison of the calculated curves and the semiempirical data to the experiment by Pecora *et al.*[18] is not very satisfactory, with the experimental spectrum being considerably broader than any other curve shown in Fig. 13. Moreover, the sharply increas-

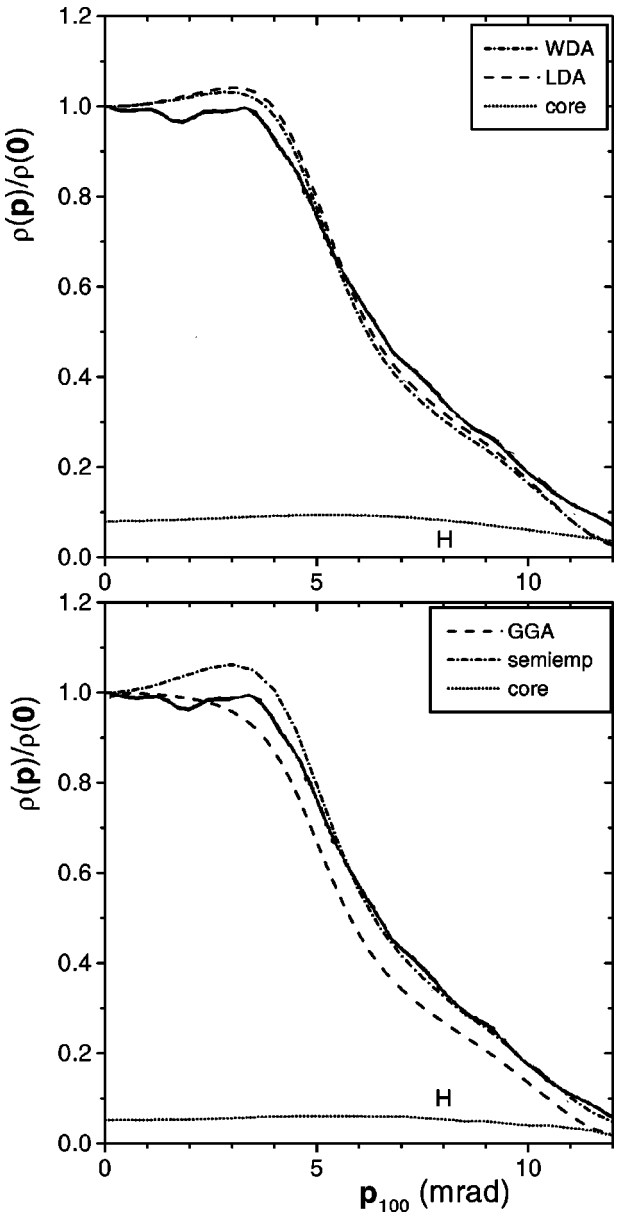

FIG. 12. Electron-positron momentum densities for V along the [100] direction, calculated within WDA, LDA-SEF, and GGA, compared to the semiempirical and experimental results. The bold lines denote the experimental 3D spectra reconstructed in Ref. 18. The semiempirical curve has been calculated according to the formulas (1) and (2) with the fitting parameters $a_s=1$, $a_p=1.2$, $a_d=1$, $b_s=0.1$, $b_p=0.2$, $b_d=0$, and $c_s=c_p=c_d=0$, taken from Ref. 6. The core electron contribution is marked by the dotted line. All the spectra are normalized to unity at $\mathbf{p}=\mathbf{0}$ and momenta are expressed in miliradians.

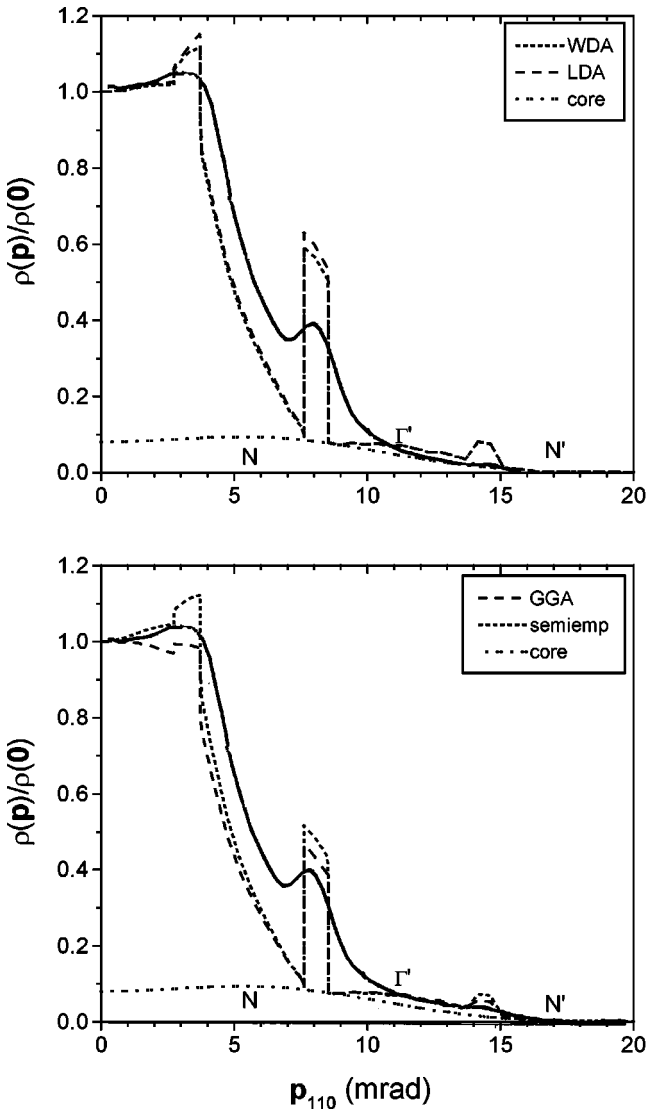

FIG. 13. Electron-positron momentum densities for V along the [110] direction, calculated within WDA, LDA-SEF, and GGA, compared to the semiempirical and experimental results. The bold lines denote the experimental 3D spectra reconstructed in Ref. 18. The semiempirical curve has been calculated according to the formulas (1) and (2) with the fitting parameters $a_s=1$, $a_p=1.2$, $a_d=1$, $b_s=0.1$, $b_p=0.2$, $b_d=0$, and $c_s=c_p=c_d=0$, taken from Ref. 6. The core electron contribution is marked by the dotted line. All the spectra are normalized to unity at $\mathbf{p}=\mathbf{0}$ and momenta are expressed in milliradians.

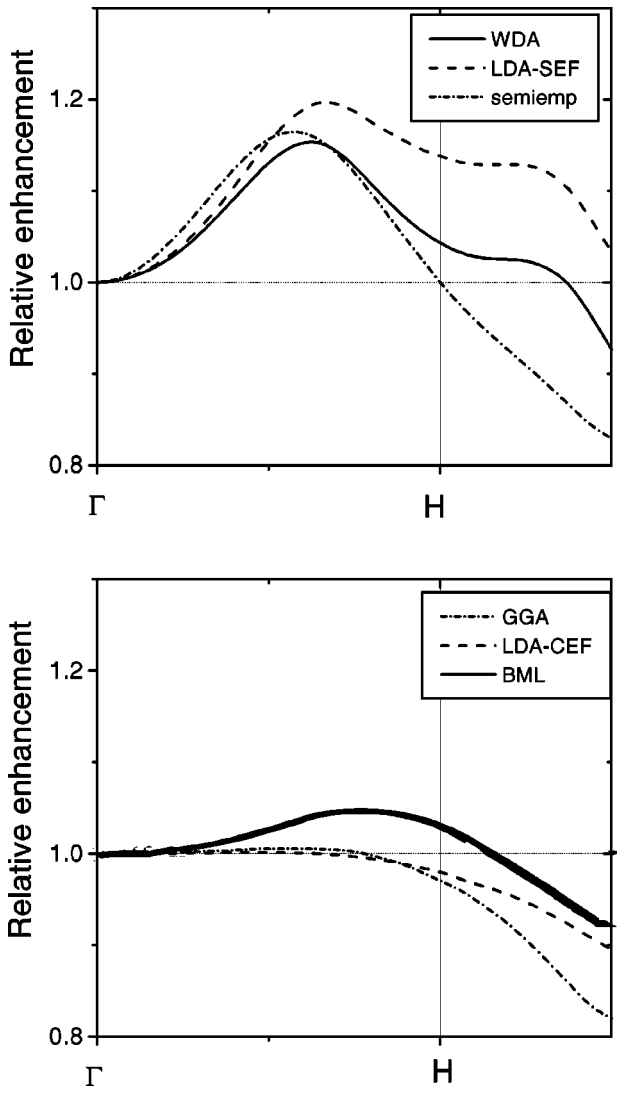

FIG. 14. Momentum-dependent relative enhancement factors, $\epsilon(\mathbf{p})/\epsilon(\mathbf{0})$, calculated within various approximations for V along the [100] direction.

ing behavior of the theoretical curves, observed close to the *N* point, is not reflected in the experimental curve. The source of these differences between theory and experiment may lie in the quality of the reconstruction technique and finite resolution of the ACAR apparatus.[18] It is encouraging, however, that although the experimental curve shows a considerably smaller ''peak to-valley'' ratio, as compared to any theoretical curve or the semiempirical data, the peak positions of both the theoretical and semiempirical curves are not shifted with respect to the experiment. It is also satisfying that the structure observed in the present WDA and LDA momentum densities is not more pronounced than that observed in other calculations.[12]

In Fig. 14, the relative *e-p* enhancement factors, $\epsilon(\mathbf{p})/\epsilon(\mathbf{0})$, along the [100] direction, for the only annihilation active band, are displayed. One can see that their behavior is strongly linked to the underlying electronic structure. All calculated enhancement factors, as well as the semiempirical curve, similar to the first annihilation active band in Cu (Fig. 9), show negative slopes in the high-momentum region. Moreover, a *deenhancement* effect is clearly visible in all annihilation characteristics. Also, WDA seems to provide better agreement with the semiempirical data than LDA-SEF, both in the low- and high-momentum space. In the first Brillouin zone, the WDA, LDA-SEF, and semiempirical results show more structure than that observed in Cu, reflecting stronger dispersion of the first annihilation active band. Note that a hump seen in the second BZ, below the *H* point, is simply the umklapp image of the ''bulge'' in the energy band. This local maximum is not observed in the

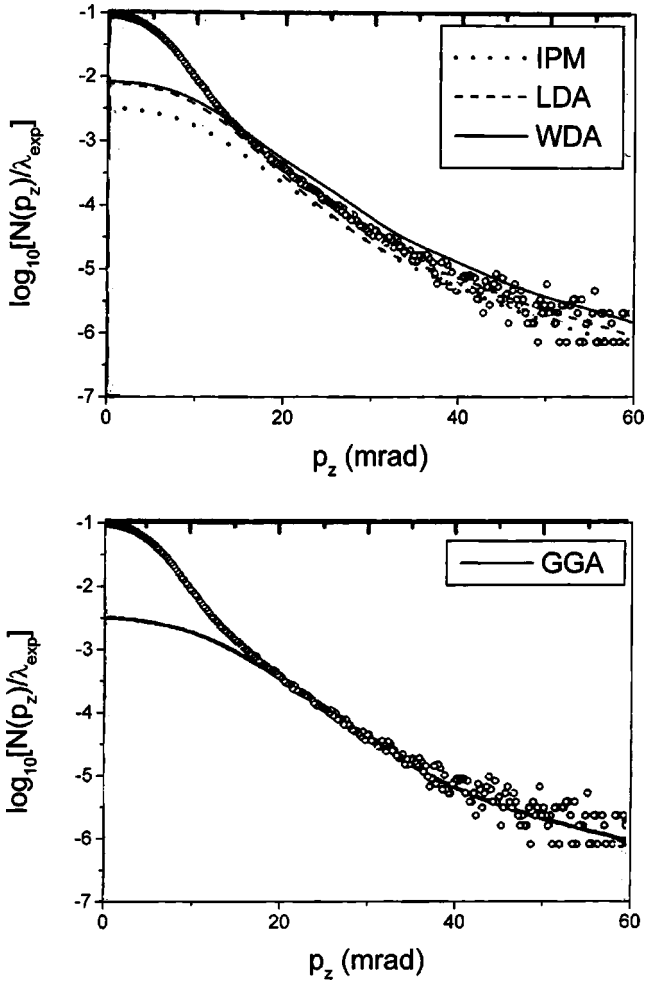

FIG. 15. Core electron annihilation probability densities $N(p_z)$ for Al, from the present calculations within the IPM, LDA, and WDA approximations, in comparison with the experimental Doppler broadening data and GGA calculation, for core electrons only, extracted by scan from the paper by Asoka-Kumar *et al.* (Ref. 24) (lower panel). The GGA curve, unlike the IPM, LDA, and WDA results, has been convoluted with a Gaussian to mimic the finite experimental resolution. Due to normalization of the experimental data to unit volume, the IPM, LDA, and WDA curves have been normalized to λ_c/λ_{exp}.

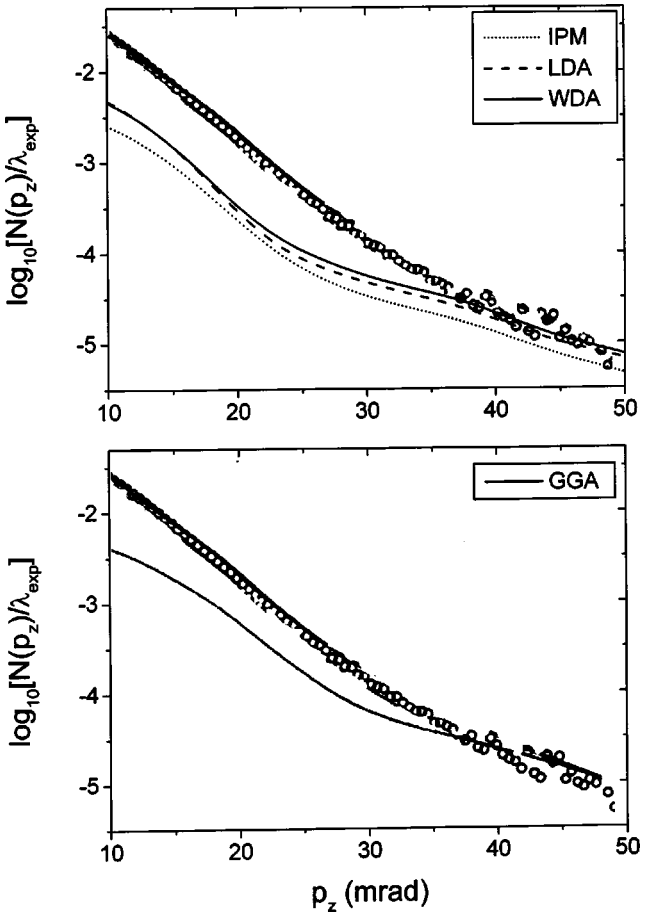

FIG. 16. Core electron annihilation probability densities $N(p_z)$ for Cu, from the present calculations within the IPM, LDA, and WDA approximations, in comparison with the experimental Doppler broadening data and GGA result, for core electrons only, extracted by scan from the paper by Barbiellini *et al.* [Ref. 15(c)] (bottom panel). The GGA curve, unlike the IPM, LDA, and WDA results, has been convoluted with a Gaussian to mimic the finite experimental resolution. Due to normalization of the experimental data to unit volume, the IPM, LDA, and WDA curves have been normalized to λ_c/λ_{exp}.

semiempirical curve, implying pure *d* character of $\rho(\mathbf{p})$ in this region. Indeed, the semiempirical correlation functions for *d* electrons are completely energy independent and, therefore, the resulting enhancement factor cannot reproduce details of the energy band slope.

The BML, GGA, and LDA-CEF enhancement factors are very similar, both quantitatively and qualitatively, to the corresponding quantities for the first annihilation active band in Cu. This behavior of the *e-p* enhancement factor is easy to understand in the case of the state-independent approaches of GGA and LDA-CEF, which are hardly sensitive to the slope of the energy band as a function of momentum. However, it is rather surprising in the case of the enhancement factors obtained within the state-dependent approach of BML. The shape of the BML enhancement factors for vanadium, along the [100] direction, is almost indistinguishable from the corresponding quantity in copper, despite the fact that the energy dispersion in the first band differs considerably between these systems. This could suggest that some important terms in the BML scattering amplitudes of the *e-p* wave function have been neglected during the BML optimization procedure.[8] Finally, note that for momenta inside the first BZ, the BML, GGA, or LDA-CEF cannot reproduce the increasing slope of the semiempirical curve in V.

E. Core electrons

In this section we briefly discuss the influence of the nonlocal *e-p* correlation effects on the one-dimensional *e-p* momentum densities

$$N(p_z)=\int_{|p_z|}^{\infty} p\rho_c(|\mathbf{p}|)dp,$$

originating from the core electron contribution, $\rho_c(|\mathbf{p}|)$, to the total e-p momentum density given by Eq. (1). The $N(p_z)$ curves, calculated within IPM, LDA, and WDA, for Al and Cu, are shown, respectively, in Figs. 15 and 16, and compared to the experimental Doppler broadening spectra and GGA calculations from Refs. 15 and 24. The most important point to be made about these results is that including the e-p correlation effects improves the agreement with the experimental data, over the IPM result. Both LDA and WDA give fairly satisfactory results, although the WDA curve runs higher than the LDA curve, for both metals. The noticeably higher values of the WDA curve for Al seem to be caused mainly by the shape of the positron wave function.[11] The latter may also be partially responsible for the observed differences between the WDA and GGA curves, although the fact that the WDA curve has not been convoluted with a Gaussian has to be kept in mind too. For Cu, on the other hand, both nonlocal approaches, WDA and GGA, appear to deliver nearly the same degree of consistency with the experimental spectrum although, as in the case of Al, the WDA curve has not been convoluted with a Gaussian to mimic the finite experimental resolution. In general, however, due to statistical errors occurring in the experimental data in the very-high-momentum region, the issue of identifying the preferred or best theoretical approximation seems to be almost immaterial here. In addition, the BML approximation, another nonlocal approach discussed in the present paper, due to its very construction, cannot be applied to evaluating the core contribution to the $N(p_z)$ densities.[8]

IV. CONCLUSIONS

In summary, we have shown that the nonlocal e-p interaction effects play essential role in the calculations of the e-p momentum densities and enhancement factors in d-electron metals, especially for momenta close to the BZ boundary and in the umklapp region. In simple metals, for momenta inside the central Fermi surface, the nonlocality of the e-p correlations is not of much importance for the positron annihilation characteristics, but the state dependence of the e-p correlation functions is important both in these systems and in transition metals.

In transition metals the *deenhancement* of $\rho(\mathbf{p})$, predicted by experiment,[1,31] is observed in the umklapp region, while in simple metals the e-p momentum density is *overenhanced*. In transition metals this effect is moderated within the local theories but is strongly enhanced by the nonlocality of the e-p interaction. In simple metals the state-dependent approach of WDA reduces the *overenhancement* effects in comparison with the local quantities, while the state-independent approach of GGA seems to increase the *overenhancement* with respect to the LDA-CEF result.

Finally, we have shown that the e-p enhancement factors strongly depend on the underlying electronic structure and in particular the dispersion of the energy bands and the character of the wave functions. The results of the present work indicate that comparison of the ACAR spectra with Compton profiles could provide some information on the d character in the electron wave function and resulting EMD. These effects are most pronounced in the high-momentum region, and we would therefore wish to encourage more experimental work in this region of momentum space. This should be feasible with the latest positron annihilation technology and would open up new avenues of obtaining from positron annihilation experiments much more information about the electronic structure than just the Fermi surface breaks.

ACKNOWLEDGMENTS

We thank Thomas Jarlborg, Stephen Dugdale, and Heinrich Sormann for useful communications. Moreover, we gratefully acknowledge the State Committee for Scientific Research (Poland) (Grant No. 2P03B 107 16) for financial support of this work.

[1] For review see, e.g., S. Berko, in *Positron Solid State Physics*, edited by W. Brandt and A. Dupasquier (North-Holland, Amsterdam, 1983), p. 64; F. Sinclair, W. S. Farmer, and S. Berko, in *Positron Annihilation*, edited by P. G. Coleman, S. C. Sharma, and L. M. Diana (North-Holland, Amsterdam, 1982), p. 322.

[2] For review see, e.g., R. N. West, *Positron Studies of Condensed Matter* (Taylor and Francis, London, 1974); M. J. Puska and R. M. Nieminen, Rev. Mod. Phys. **66**, 841 (1994); R. M. Nieminen, in *Positron Spectroscopy of Solids*, edited by by A. Dupasquier and A. P. Mills Jr. (IOS Press, Amsterdam, 1995), p. 443.

[3] S. M. Kim and A. T. Stewart, Phys. Rev. B **11**, 2490 (1975); T. Hyodo, T. McMullen, and A. T. Stewart, in *Positron Annihilation*, Ref. 1, p. 201; P. Kubica and A. T. Stewart, Phys. Rev. Lett. **34**, 852 (1975).

[4] P. E. Mijnarends and R. M. Singru, Phys. Rev. B **19**, 6038 (1979); M. Šob, J. Phys. F: Met. Phys. **12**, 571 (1982).

[5] B. Chakraborty, Phys. Rev. B **24**, 7423 (1981); in *Positron Annihilation*, Ref. 1, p. 207.

[6] P. Genoud, A. K. Singh, A. A. Manuel, T. Jarlborg, E. Walker, M. Peter, and M. Weller, J. Phys. F: Met. Phys. **18**, 1933 (1988); P. Genoud, Ph.D. thesis, Geneva University (1990); A. A. Manuel, A. K. Singh, T. Jarlborg, P. Genoud, L. Hoffmann, and M. Peter, in *Positron Annihilation*, edited by L. Dorikens-Vanpraet, M. Dorikens, and P. Seegers (World Scientific, Singapore, 1989), p. 109.

[7] J. P. Carbotte, in *Positron Solid State Physics* (Ref. 1, p. 32); H. Sormann and W. Puff, in *Positron Annihilation*, edited by P. C. Jain, R. M. Singru, and K. P. Gopinathan (World Scientific, Singapore, 1985), p. 161.

[8] H. Sormann, Phys. Rev. B **54**, 4558 (1996).

[9] S. Daniuk, G. Kontrym-Sznajd, A. Rubaszek, H. Stachowiak, J. Mayers, P. A. Walters, and R. N. West, J. Phys. F: Met. Phys. **17**, 1365 (1987); S. Daniuk, M. Šob, and A. Rubaszek, Phys. Rev. B **43**, 2580 (1991).

[10] G. Kontrym-Sznajd and A. Rubaszek, Phys. Rev. B **47**, 6950 (1993); **47**, 6960 (1993).

[11] A. Rubaszek, Z. Szotek, and W. M. Temmerman, Phys. Rev. B **58**, 11 285 (1998); **61**, 10 100 (2000).

[12] A. K. Singh and T. Jarlborg, J. Phys. F: Met. Phys. **15**, 727 (1985); T. Jarlborg and A. K. Singh, Phys. Rev. B **36**, 4660 (1987).

[13] S. Kahana, Phys. Rev. **129**, 1622 (1963).

[14] R. M. Nieminen, in *Positron Solid State Physics*, Ref. 1; E. Boroński and R. M. Nieminen, Phys. Rev. B **34**, 3820 (1986).

[15] (a) B. Barbiellini, M. J. Puska, T. Torsti, and R. M. Nieminen, Phys. Rev. B **51**, 7341 (1995); (b) B. Barbiellini, M. J. Puska, T. Korhonen, A. Hajru, T. Torsti, and R. M. Nieminen, *ibid.* **53**, 16 201 (1996); (c) B. Barbiellini, M. Hakala, M. J. Puska, and R. M. Nieminen, *ibid.* **56**, 7136 (1997).

[16] H. Kondo, T. Kubota, H. Nakashima, and S. Tanigawa, Mater. Sci. Forum **105-110**, 675 (1992).

[17] H. Nakashima, T. Kubota, Y. Murakami, H. Kondo, and S. Tanigawa, Mater. Sci. Forum **105-110**, 779 (1992).

[18] L. M. Pecora, J. Phys.: Condens. Matter **1**, SA1 (1989); L. M. Pecora, A. C. Ehrlich, A. A. Manuel, A. K. Singh, and R. M. Singru, in *Positron Annihilation*, Ref. 7, p. 254; Phys. Rev. B **37**, 6772 (1988).

[19] P. Hohenberg and W. Kohn, Phys. Rev. **136**, B364 (1964); W. Kohn and L. J. Sham, *ibid.* **140**, A133 (1965).

[20] O. K. Andersen, Phys. Rev. B **12**, 3060 (1975); W. R. L. Lambrecht and O. K. Andersen, *ibid.* **34**, 2439 (1986).

[21] R. M. Nieminen and M. J. Puska, Phys. Rev. Lett. **50**, 281 (1983); R. M. Nieminen, M. J. Puska, and M. Manninen, *ibid.* **53**, 1298 (1984); M. J. Puska and R. M. Nieminen, J. Phys. F: Met. Phys. **13**, 2695 (1983).

[22] M. J. Puska, J. Phys.: Condens. Matter **3**, 3455 (1991); F. Plazaola, A. P. Seitsonen, and M. J. Puska, *ibid.* **6**, 8809 (1994).

[23] W. Brandt and J. Reinheimer, Phys. Lett. A **35**, 109 (1971); J. Arponen and E. Pajanne, J. Phys. C **12**, 3013 (1979). Function $\gamma^h(n_0)$ was parametrized by Barbiellini *et al.* (Ref. 15); J. Arponen and E. Pajanne, J. Phys. F: Met. Phys. **9**, 2359 (1979), provided momentum-dependent enhancement factors $\epsilon^h((E/E_F),n_0)$; A. Kallio, P. Pietiläinen, and L. Lantto, Phys. Scr. **25**, 943 (1982). Function $\gamma^h(n_0)$ was parametrized by Boroński and Nieminen (Ref. 14). Function $\gamma^h(n_0)$ and enhancement factors $\epsilon^h((E/E_F),n_0)$ were parametrized by H. Stachowiak and J. Lach, Phys. Rev. B **48**, 9828 (1993); also see H. Stachowiak, *ibid.* **41**, 12 522 (1990).

[24] M. Alatalo, H. Kauppinen, K. Saarinen, M. L. Puska, J. Makinen, P. Hautojärvi, and R. M. Nieminen, Phys. Rev. B **51**, 4176 (1995); M. Alatalo, H. Kauppinen, M. J. Puska, K. Saarinen, J. Mäkinen, P. Hautojärvi, and R. M. Nieminen, *ibid.* **54**, 2397 (1996); V. J. Ghosh, M. Alatalo, P. Ashoka-Kumar, B. Nielsen, and K. G. Lynn, *ibid.* **61**, 10 092 (2000); P. Asoka-Kumar, M. Alatalo, V. J. Ghosh, A. C. Kruseman, B. Nielsen, and K. G. Lynn, Phys. Rev. Lett. **77**, 2097 (1996).

[25] A. Seeger, F. Banhart, and W. Brauer, in *Positron Annihilation*, Ref. 6, p. 275.

[26] A. Baranowski and E. Dębowska, Appl. Phys. A: Mater. Sci. Process. **51**, 23 (1990); Acta Phys. Pol. A **88**, 13 (1995).

[27] A. Rubaszek and H. Stachowiak, Phys. Status Solidi B **124**, 159 (1984); Phys. Rev. B **38**, 3846 (1988); A. Rubaszek, H. Stachowiak, E. Boroński, and Z. Szotek, *ibid.* **30**, 2490 (1984) provide momentum-dependent enhancement factors $\epsilon^h((E/E_F),n_0)$.

[28] L. Pecora and A. C. Ehrlich, Phys. Rev. B **19**, 719 (1979).

[29] P. Harthoorn and P. E. Mijnarends, J. Phys. F: Met. Phys. **8**, 1147 (1978).

[30] C. K. Majumdar, Phys. Rev. **140**, A227 (1963).

[31] S. Wakoh, S. Berko, M. Haghooie, and J. J. Mader, J. Phys. F: Met. Phys. **9**, L231 (1979).

[32] T. Kubota, H. Nakashima, H. Kondo, S. Tanigawa, Y. Murakami, Y. K. Cho, and G. W. Bahng, Mater. Sci. Forum **105-110**, 723 (1992).